

Room Temperature Methane Capture and Activation by Ni Clusters Supported on TiC(001): Effects of Metal-Carbide Interactions on the Cleavage of the C-H Bond

Hèctor Prats[†], Ramón A. Gutiérrez^{‡,x}, Juan José Piñero[†], Francesc Viñes[†], Stefan T. Bromley,^{†§}
Pedro J. Ramírez^x, José A. Rodríguez^{*,‡} and Francesc Illas^{*,†}

[†]*Departament de Ciència de Materials i Química Física & IQTCUB, Universitat de Barcelona, Martí i Franquès 1-11, 08028 Barcelona, Spain.*

[‡]*Chemistry Department, Brookhaven National Laboratory, Upton, New York 11973, USA.*

^x*Facultad de Ciencias, Universidad Central de Venezuela Caracas 1020-A, Venezuela.*

[§]*Institució Catalana de Recerca i Estudis Avançats (ICREA), Barcelona, Spain.*

ABSTRACT

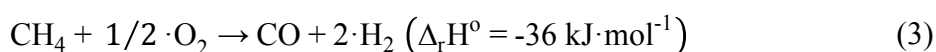
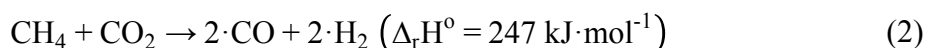
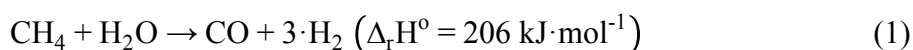
Methane is an extremely stable molecule, a major component of natural gas, and also one of the most potent greenhouse gases contributing to global warming. Consequently, the capture and activation of methane is a challenging and intensively studied topic. A major research goal is to find systems that can activate methane even at low temperature. Here, combining ultrahigh vacuum catalytic experiments followed by X-ray photoemission spectra and accurate density functional theory (DFT) based calculations, we show that small Ni clusters dispersed on the (001) surface of TiC are able to capture and dissociate methane at room temperature. Our DFT calculations reveal that two-dimensional Ni clusters are responsible of this chemical transformation, evidencing that the lability of the supported clusters appears to be a critical aspect in the strong adsorption of methane. A small energy barrier of 0.18 eV is predicted for CH₄ dissociation into adsorbed methyl and hydrogen atom species. In addition, the calculated reaction free energy profile at 300 K and 1 atm of CH₄ shows no effective energy barriers in the system. Comparing with other reported systems which activate methane at room temperature, including oxide and zeolite-based materials, indicates that a different chemistry takes place on our metal/carbide system. The discovery of a carbide-based surface able to activate methane at low temperatures paves the road for the design of new types of catalysts towards an efficient conversion of this hydrocarbon into other added-value chemicals, with implications in climate change mitigation.

* Corresponding authors: José A. Rodríguez (rodriguez@bnl.gov), Francesc Illas (francesc.illas@ub.edu)

INTRODUCTION

Although carbon dioxide (CO₂) is the main greenhouse gas, in terms of its overall contribution to global warming, methane (CH₄), the simplest, most abundant and stable alkane molecule, immediately follows.¹ Even though CH₄ emissions are five times smaller than CO₂, its greenhouse effect is 23 times larger, and, therefore, its contribution to climate change comparable to that of CO₂. The Earth's atmospheric methane content has oscillated between 350 and 800 volumetric parts per billion (*ppb*) during the last glacial and interglacial periods,² with main release sources being wetlands, living organisms, and permafrost melting processes.³ However, since the industrial revolution, CH₄ levels have risen to the present value of 1770 *ppb*,^{4,5} mostly from anthropogenic sources, including unsustainable landfills, livestock farming, and fossil fuels used for energy production and transportation.⁶⁻⁸

Different combined strategies oriented towards reducing the content of greenhouse gases in the atmosphere include: reducing emissions, more efficient use of fossil fuel sources of energy, using alternative renewable, green sources of energy. A particularly appealing strategy is to use carbon capture and storage (CCS) technologies⁹ where appropriate, specific, materials are used as CO₂ or CH₄ scrubbers. Even more interesting are carbon capture and usage (CCU) technologies, where the corresponding molecules, once adsorbed, are converted, ideally catalysed by the same substrate material, into other valuable chemicals.¹⁰ In the case of captured methane this is a real challenge because of the high 4.5 eV C-H bond strength, the absence of low-energy empty orbitals, and the presence of high energy occupied orbitals.⁷ An ideal transformation process would involve the production of synthesis gas (*syngas* for short) —a gas stream mixing carbon monoxide (CO) and hydrogen (H₂). This syngas can be used as feedstock for Fischer-Tropsch synthesis, after H₂ enrichment or diminution, to obtain long-chain hydrocarbons.¹¹ The syngas stream formation can pass through different reactions, including methane dry reforming (Eq. 1),¹²⁻¹⁴ methane steam reforming (Eq. 2),^{11,15,16} or methane partial oxidation (Eq. 3).¹⁷⁻¹⁹



The common limiting steps for such processes are, first, methane adsorption, and, second, its subsequent activation. These steps are intimately related to the first hydrogen

abstraction from CH₄, which is regarded as the rate determining step of the overall mechanism.²⁰⁻²² In addition, methane also can be transformed directly into commodity chemicals such as methanol, ethylene, or benzene.⁷ An optimal catalyst for CH₄ capture and conversion would be one that simultaneously meets two criteria, namely: *i*) it must adsorb CH₄ —ideally even at room temperature, and *ii*) it must feature a low enough energy barrier for C-H bond scission —preferably to be overcome at room temperature as well. On a reaction free energy profile, these criteria would imply that the first dehydrogenation reaction step transition state would be lower than the molecular desorbed state.

There is an ongoing search for materials that can accomplish the activation of methane at low temperatures to enable the direct conversion of CH_x fragments into commodity chemicals.⁷ Most of the studies dealing with the activation of methane have focussed their attention on metals, bulk oxides, homo- and hetero-nuclear oxide clusters, zeolites, and also on biomimetic approaches.^{7,21-25} On metal surfaces, methane binds weakly and the probability for dissociation is low.²⁶ Reactions 1-3 above are nowadays carried out at elevated temperatures on Ni-based catalysts.^{11,20} A previous DFT study regarding the Ni(111) surface explains this fact in the sense that the first C-H bond scission is endothermic by 0.36 eV and involves an energy barrier (E_b) of 1.07 eV.²⁷ Similar calculations for CH₄ on Pt(111) show the process to be energetically uphill by 0.17 eV with a slightly reduced energy barrier of 0.93 eV. This result is in line with the experimental observation of a barrier reduction of 0.29 ± 0.06 eV when comparing CH₄ reactivity on Pt(111) to that exhibited by Ni(111).²⁸ Nevertheless, metals are not, in general, very efficient for C-H bond cleavage.²⁴⁻³⁰

A few oxide and metal/oxide systems can activate methane at low temperature.^{21,22,31,32} On these materials, it has been found that cooperative interactions between a cation and an oxide centre can lead to a cleavage of the first C-H bond in methane with energy barriers that are below 0.5 eV. In this aspect, these oxide-based systems are more efficient than metals or metal alloys. In this study, we move in a different direction and, by combining X-ray Photoemission Spectroscopy (XPS) experiments with state-of-the-art DFT based calculations, show that small Ni particles in contact with a metal carbide such as TiC can also trigger the cleavage of C-H bonds at 300 K. This is a remarkable finding since both bulk Ni and TiC exhibit very low activity towards methane activation. Clearly, there is a synergy in the Ni/TiC(001) system that facilitates the activation of methane. In this way, the present work points to

a new approach for developing a novel family of materials that would be active for CH₄ activation under mild conditions.

EXPERIMENTAL DETAILS

The reactivity of Ni/TiC(001) surfaces towards methane was studied in a system which combines an ultrahigh-vacuum (UHV) chamber (base pressure $\sim 7 \cdot 10^{-10}$ mbar) and a batch reactor.³³⁻³⁶ Within this system, the sample could be transferred between the reactor and UHV chamber without exposure to air. The UHV chamber was equipped with instrumentation for X-ray and ultraviolet photoelectron spectroscopies (XPS and UPS), low-energy electron diffraction (LEED), ion scattering spectroscopy (ISS), and temperature-programmed desorption (TPD).

The TiC(001) single crystal was cleaned following methodologies reported in the literature.^{37,37} Nickel was vapour-deposited on the TiC(001) surface at 300 K.³⁷ The admetal doser consisted of a resistively heated tungsten basket with a drop of ultrapure Ni inside.³⁷ Initially the flux of the doser was calibrated by taken thermal desorption spectra for the desorption of Ni from a Mo(100) substrate.^{33,38} This information was then used to calibrate admetal coverages estimated by means of XPS.³³

In the tests of methane activation, the Ni/TiC(001) samples were transferred to the reactor at ~ 300 K, then 1.33 mbar (1 Torr) of methane was introduced for a period of five minutes. After this exposure, the methane gas was removed and each sample was transferred back to the UHV chamber for surface characterization. Maximum activity was found for small coverages, 0.2-0.3 monolayers (ML), of nickel on the carbide substrate.

COMPUTATIONAL METHODS

As explained above, both Ni(111) and TiC(001) are inactive whereas CH₄ maximum conversion is observed for small dosages of 0.2-0.3 ML of Ni over the TiC(001) surface. This suggests that small supported Ni clusters are the main players, in accordance with previous studies of Au and Cu clusters on TMCs.³⁹⁻⁴¹ Consequently, CH₄ activation on Ni/TiC(001) is assessed by modelling different types of TiC-supported Ni clusters using periodic DFT based calculations. Specifically, the pristine TiC(001) surface, three different Ni_n/TiC(001) ($n = 4, 9, 13$) clusters (see Figure 1), and a Ni supported nanorod model (see Figure 2) featuring low coordinated sites were investigated. These particular Ni clusters sizes have been selected as they feature a compact packaging with high symmetry, which makes them, *a priori*, very stable, thus

maximizing the atomic coordination. The calculations employed the Perdew-Burke-Ernzerhof (PBE)⁴² exchange-correlation (xc) functional, and the contribution of dispersion (vdW) terms was included through the D3 correction as proposed by Grimme (PBE-D3).⁴³ For the systems containing Ni NCs, as well as for gas phase CH₃ and H (see below), spin polarization was taken explicitly into account. The transition states (TS) were located using the climbing-image NEB (CI-NEB) method.⁴⁴ Initial guesses for the five employed intermediate images were generated by means of the Atomic Simulation Environment (ASE)⁴⁵ using the Image Dependent Pair Potential (IDPP).⁴⁶ The energy reaction profiles were obtained at 0 K and in vacuum but also at working conditions of temperature and CH₄ partial pressure by using the atomistic thermodynamics approach.⁴⁷ All calculations were carried out using the Vienna *Ab Initio* Simulation Package (VASP) code.⁴⁸ Further computational details are provided in the Supplementary Information (SI). Favourable adsorption energies, E_{ads} , are defined negative.

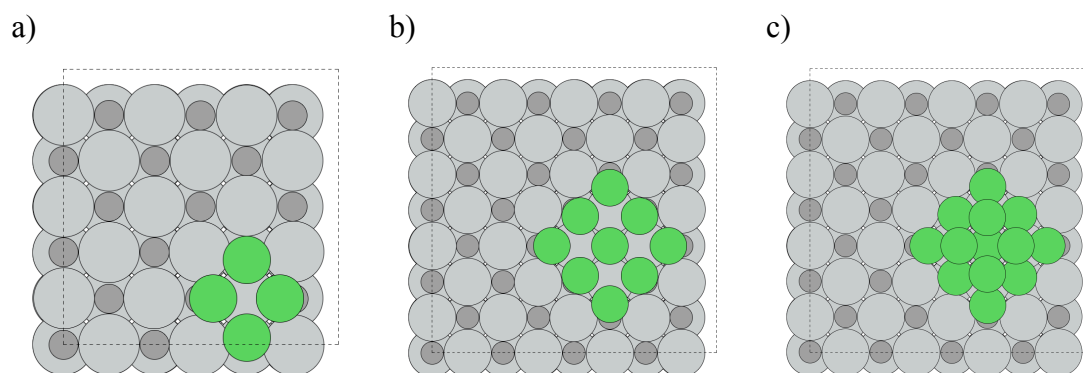


Figure 1. Most stable optimized geometries found for (top view, PBE-D3) of a) Ni₄/TiC, b) Ni₉/TiC, and c) Ni₁₃/TiC. Ni atoms are shown as green spheres, and Ti and C atoms as light and dark grey spheres, respectively. The unit cell is shown by black dotted lines.

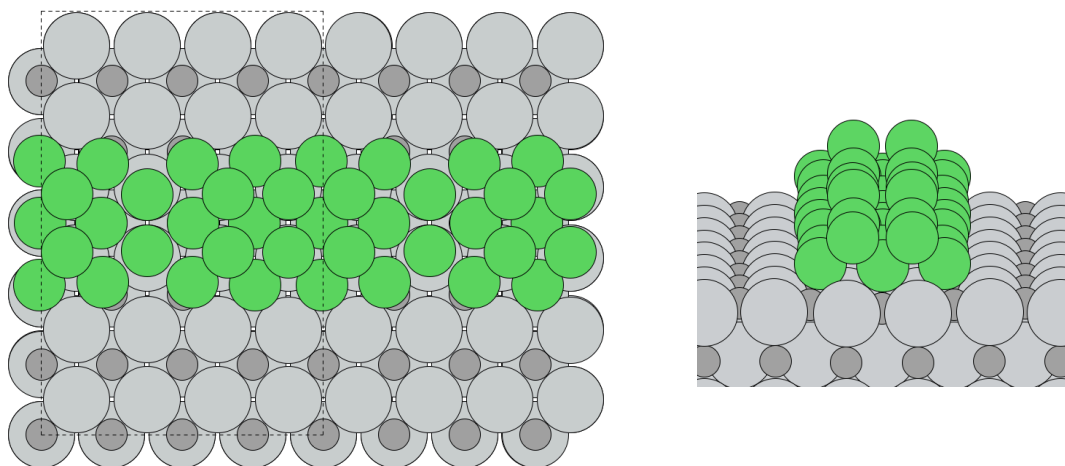


Figure 2. Optimized geometries (top and near-side views) of the Ni rod. Ni atoms are shown as green spheres, and Ti and C atoms as light and dark grey spheres, respectively. The unit cell is shown in black dotted lines.

RESULTS AND DISCUSSION

Experiments. In our experiments, surfaces of Ni/TiC(100), TiC(001) and Ni(111) were exposed to methane in a batch reactor. Figure 3 shows C 1s XPS spectra collected after dosing to methane a TiC(001) surface pre-covered with 0.2 ML of nickel (top panel) and bare Ni(111) (bottom panel). In agreement with previous studies,²⁶ we found no adsorption of methane after exposing Ni(111) and TiC(001) to 1.33 mbar (1 Torr) of the molecule at 300 K. The adsorption and dissociation of methane on Ni/TiC(001) produces a peak at ~ 284 eV that can be attributed to adsorbed CH₃ or CH₂ species.³². We estimate that 0.2-0.3 ML of CH_x are deposited on the surface as a consequence of dissociation of methane on the Ni particles or the nickel-carbide interface. The ratio of CH_x species to Ni adatoms was in the range of 1-1.5. Figure 4 shows Ni 2p_{3/2} XPS spectra recorded for a Ni/TiC(001) surface before and after adsorption of the CH_x species produced by the dissociation of CH₄ at 300 K. Reaction with methane induced an attenuation in the signal of nickel (36 %) and a positive shift of ~ 0.4 eV in the Ni 2p_{3/2} peak. Thus, the CH_x deposited on the Ni/TiC(001) surface is in direct contact with the nickel.

We also found that the amount of Ni present on the carbide surface had a strong effect on the reactivity of the surface towards methane. Figure 5 displays the change of the CH_x intensity (peak at ~ 284 eV) as a function of Ni coverage in Ni/TiC(001). In

these experiments, all the surfaces were exposed to 1 Torr of methane for 5 minutes at 300 K. A maximum of activity is seen at Ni coverages of 0.2-0.3 ML. Under these conditions, small particles of nickel interact strongly with the TiC substrate.³³ An increase in the Ni coverage increases the size of the Ni particles, favouring Ni-Ni interactions over Ni-TiC interactions, and the admetal nanoparticles slowly acquire the chemical properties of bulk nickel losing their reactivity towards methane. At large coverages of nickel, the dissociation of methane was negligible as seen on plain Ni(111).²¹

Temperature had a strong effect on the stability of the adsorbed CH_x groups. In the XPS experiments, we observed the gradual disappearance of the CH_x species when the temperature was raised from 320 to 420 K, see Figure 6. Using a mass spectrometer we detected mainly the evolution of CH₄ from the CH_x/Ni/TiC(001) surface between 340 and 410 K, with weaker signals for C₂H₆ and C₂H₄ (see Figure 7). Thus, it is clear that the species produced by dissociation of methane are chemically active and can be used for producing more complex hydrocarbons. Relatively weak interactions between CH_x and Ni are reflected in the Ni 2p XPS results shown in Figure 4 where the intensity and position of the Ni 2p_{3/2} peak are recovered after desorbing the CH_x groups by heating to 450 K. We did not observe any decrease in the reactivity of the surface after five cycles of adsorption-desorption. In CH_x/Ni/TiC(001), one has strong Ni↔TiC interactions and moderate Ni↔CH_x interactions when the Ni coverages are below 0.3 ML.

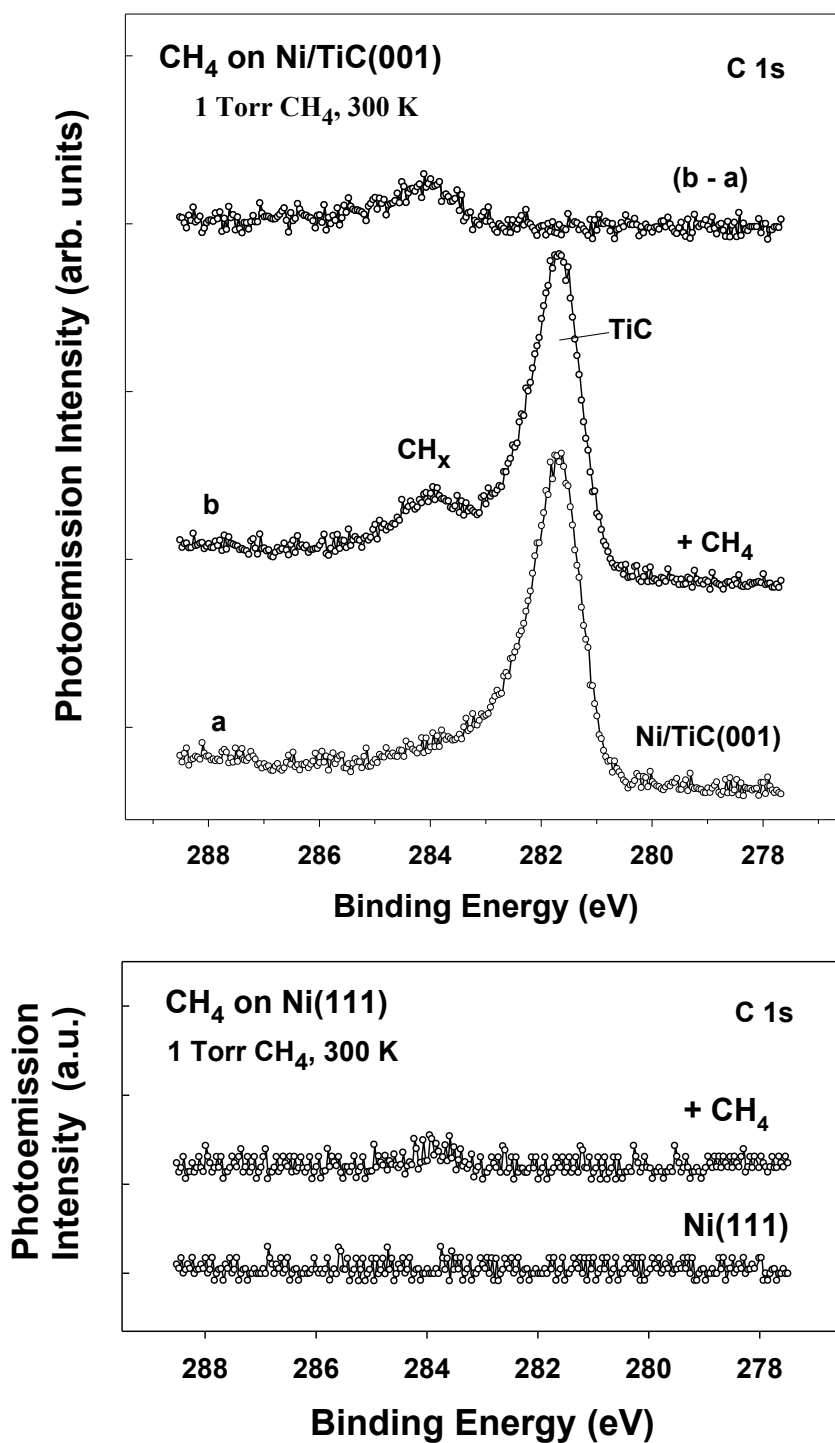


Figure 3. C 1s XPS spectra collected before and after dosing methane to Ni/TiC(001) and Ni(111) surfaces at 300 K (top and bottom panels, respectively). The dosage of methane was 1 Torr for 5 minutes. The coverage of Ni on the TiC(001) substrate was 0.2 ML.

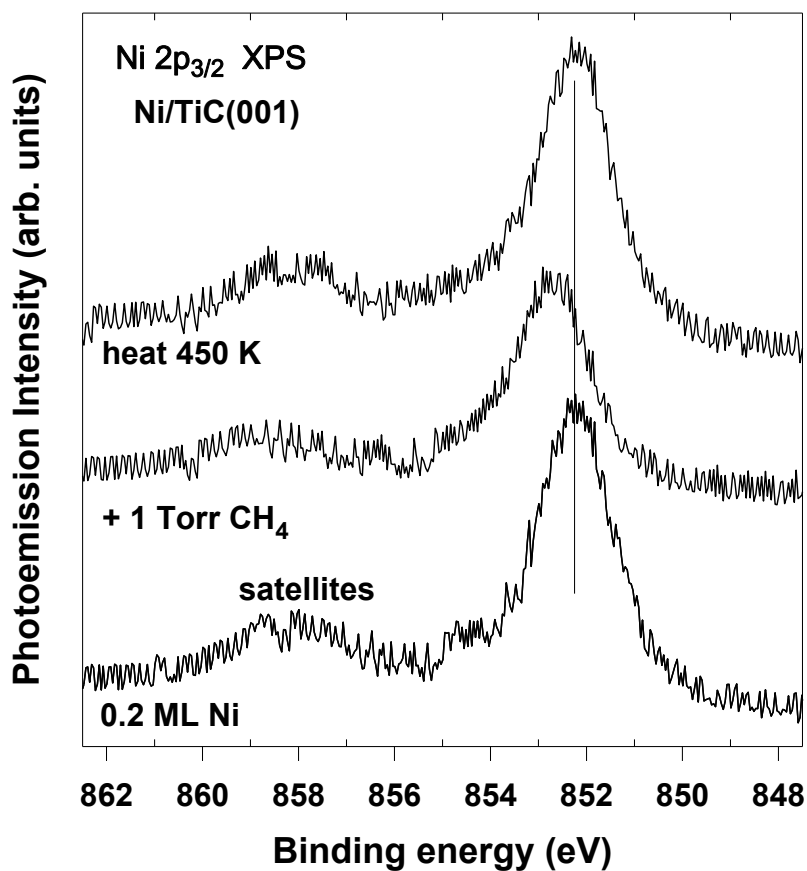


Figure 4. Ni 2p_{3/2} XPS spectra collected before and after adsorbing methane on a TiC(001) surface pre-covered with 0.2 ML of nickel. In the first step the surface was exposed to 1 Torr of methane at 300 K for 5 minutes in a batch reactor. After pumping the gas and recording the spectrum in the middle of the figure, the CH_x/Ni/TiC(001) system was heated to 450 K to induce desorption of the adsorbed CH_x species.

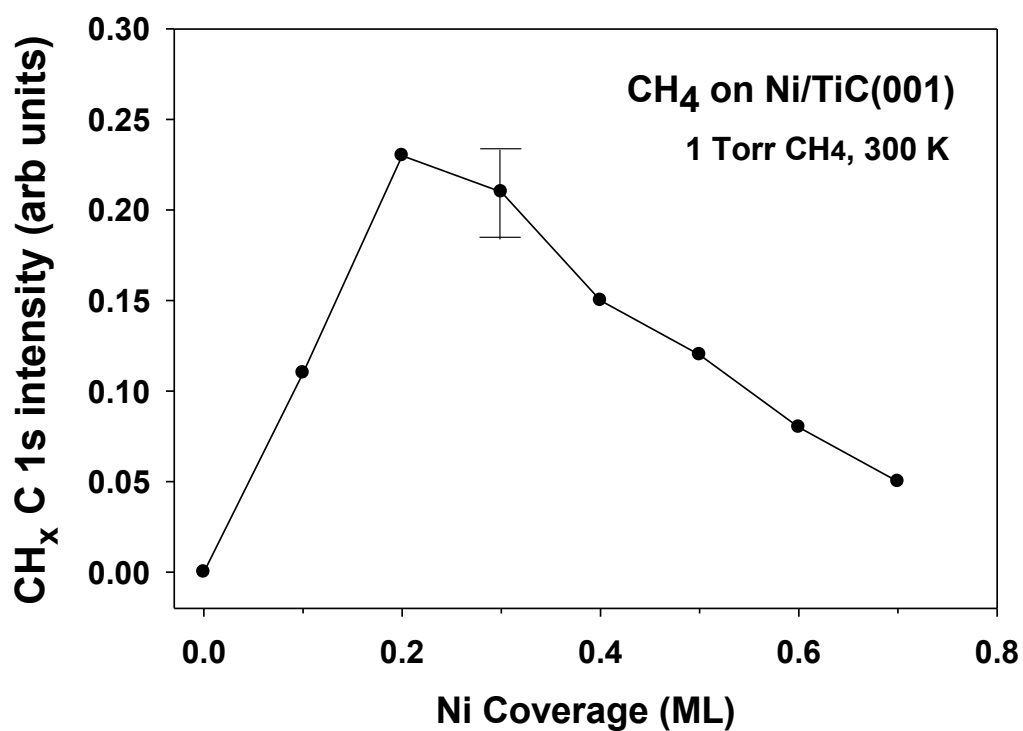


Figure 5. Variation of the CH_x intensity as a function of Ni coverage in Ni/TiC(001). In all cases the surface was exposed to 1 Torr of methane for 5 minutes at 300 K. This type of experiment was done three times and average values are reported with the typical variation for the measurements in the CH_xC 1s intensity.

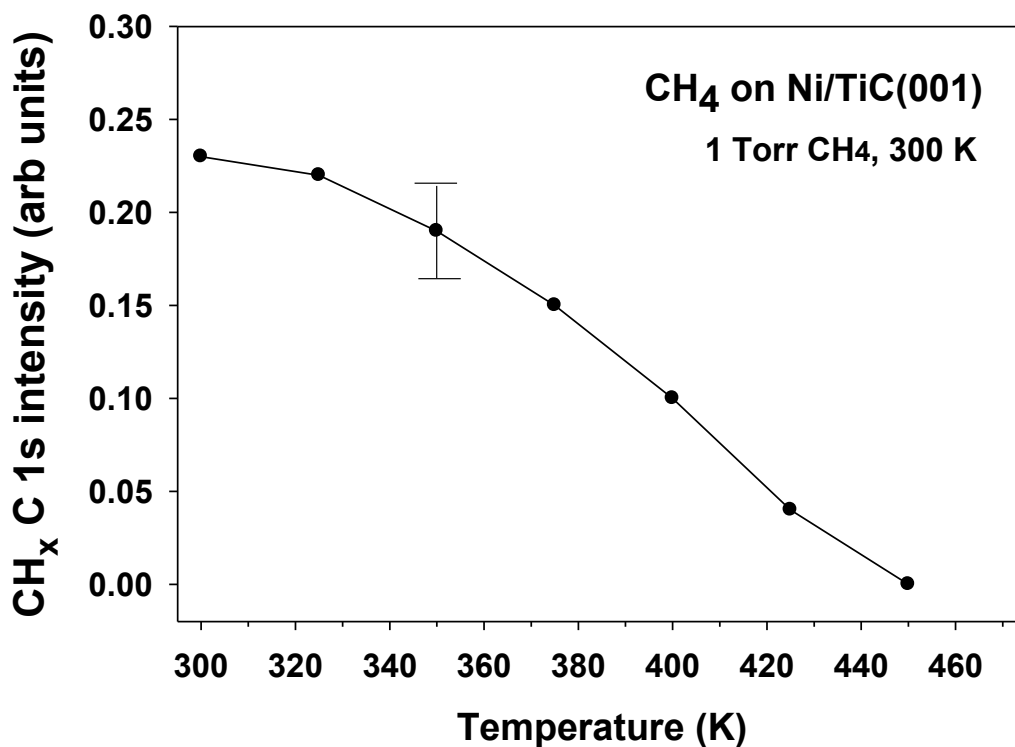


Figure 6. Effect of temperature on the C 1s signal for the CH_x species obtained after dosing methane to Ni/TiC(001) (θ_{Ni} of ~ 0.2 ML). Initially, the Ni/TiC(001) surface was exposed to 1 Torr of methane for 5 minutes at 300 K. The gas was pumped out and the temperature of the sample was ramped up under ultrahigh vacuum conditions. This type of experiment was done five times and average values are reported with the typical variation for the measurements in the CH_x C 1s intensity. In these experiments, we did not observe signs for deactivation of Ni/TiC(001).

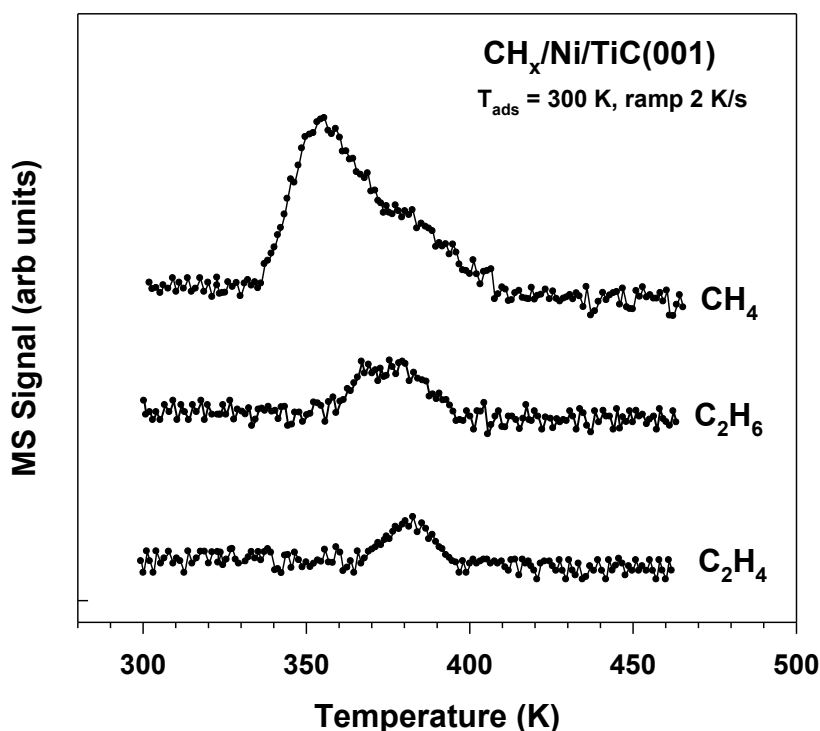


Figure 7. Temperature programmed desorption (TPD) spectra for the evolution of methane, ethane and ethylene from a CH_x/Ni/TiC(001) surface. A TiC(001) surface pre-covered with 0.2 ML of Ni was exposed to 1 Torr of methane at 300 K in a microreactor. The gas was pumped out and the sample was transferred to a UHV chamber for a TPD study (heating ramp 2 K/s).

Computational Study. To better understand the above described experiments for the Ni/TiC(001) systems, CH₄ adsorption and dissociation were studied on three Ni_n clusters (representing small to medium coverages of the admetal) and over a nano-rod (representing a large coverage of the admetal), all supported on a slab model of TiC(001). For comparison, CH₄ adsorption and dissociation on the pristine TiC(001) surface was also considered. In the latter reference case, a previous study reported a CH₄ adsorption energy of -0.25 eV,⁴⁹ similar to the value of -0.24 eV for the Ni(111) surface obtained using DFT calculations employing the PBE functional with the Grimme D2 correction.⁵⁰ The C-H bond scission of CH₄ on TiC(001) is energetically downhill although it features a large E_b of 1.5 eV (Figure 6); a similar value of 1.07 eV has been reported for the case of CH₄ dissociation on the Ni(111) surface.²⁷ The most stable CH₃ and H adsorption sites and modes are reported in Section S2 of the SI and

the TS structures for CH₄ dissociation on the clean TiC(001) are reported in Section S3. Both, TiC(001) and Ni(111) are able to adsorb methane but both feature a high C-H bond breaking energy barrier well above that of the desorption limit, thus inhibiting any further reaction as inferred from the energy (E) and Gibbs free energy (G) profiles in Figure 8.

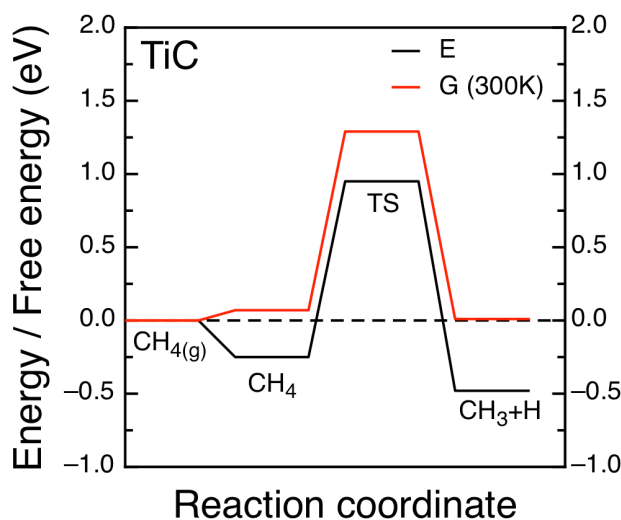


Figure 8. ZPE corrected energy profiles (E, black lines) and Gibbs free energy profiles (G) at 300 K, 1 atm of CH₄ (red lines) for CH₄ adsorption and subsequent dissociation on the clean TiC(001) surface.

With respect to the bare TiC(001) and Ni(111) surfaces, the CH₄ dissociation reaction profile on the TiC(001)-supported Ni_n clusters completely changes. The smallest Ni₄/TiC cluster features a high degree of lability since it easily stretches or contracts upon interaction with CH₄, CH₃ or H. Such easiness of deformation gradually vanishes for the larger Ni₉ and Ni₁₃ clusters. The structure of Ni₄ and Ni₉ clusters is planar whereas Ni₁₃ exhibits a three-dimensional capped pyramid structure which allows us to assess the effect of dimensionality on the CH₄ adsorption and dissociation.

On the TiC-supported Ni_n clusters, the surface sites that interact most strongly with CH₄, CH₃, and H moieties have been identified by a systematic computational screening carried out within the PBE-D3 approach. Results show that CH₄ adsorbs on all supported Ni optimized structures with adsorption energy (E_{ads}) of ~ 0.3 eV, whereas CH₃ and H exhibit larger E_{ads} values of ~ 2.5 eV. The most favourable adsorption situations and corresponding E_{ads} values are collected in Table 1. The structure of all considered sites, the adsorption energy values and optimized geometries for the most stable cases can be found in Sections S3 and S4 of the SI. Results show that on the

Ni_n/TiC systems, the CH₄ adsorption energy is 1.5-2.5 times stronger than on the clean TiC(001) surface. Notice that CH₄ prefers to adsorb on low coordinated Ni atoms (*i.e.*, on the vertices of the clusters, see Figure S4), rather than on the TiC substrate near the Ni cluster boundary region. Furthermore, CH₄ adsorption on the 3D supported Ni₁₃ cluster is noticeably weaker than for the planar 2D Ni₄ and Ni₉ cases. As the size of the Ni cluster increases, its reactivity towards CH₄ and CH₃ decreases, in agreement with the experimental trend seen in Figure 5. The highest reactivity is found on the Ni₄/TiC(001) system, where all the Ni adatoms are in contact with the carbide surface and have a few metal neighbours. At this point one may wonder about the origin of such enhanced activity of Ni₄ clusters when supported on TiC(001), and whether this is instigated by a particular electronic structure. Such enhanced activity and reactivity observed on Ni₄ clusters supported on TiC(001) has been observed in the past in similar systems, such as Au₄ clusters supported on TiC(001) catalysts, active in desulfurization reactions,^{39,51,52} as well as Cu₄, Ni₄, and Au₄ clusters supported on TiC(001) which exhibit activity towards CO₂ hydrogenation reactions.³⁶ Detailed experiments and theoretical modelling have shown that the underlying chemistry of transition metal clusters supported on carbides such as TiC arises from the substrate induced electron density polarization of the supported metal clusters, with no evidence of net charge transfer. This is in agreement with experimental and computational evidence confirming that the enhanced activity/reactivity is larger for small flat metal clusters, and tends to vanish in larger, three-dimensional metal clusters and nanoparticles.^{53,54} Such polarization does not seem to be exclusive to TMCs, as, in a similar way, a recent study by Li *et al.* reported that the large spin polarization of Fe₃ clusters supported on Al₂O₃ is responsible for the activation of N₂ in the conversion of N₂ to NH₃.⁵⁵

However, aside from the electron density polarization reported for other related systems, the relatively high lability of the smallest Ni₄ supported cluster deserves some additional comments. The cluster elongates in the direction where one Ni atom interacts with CH₄, and contracts adopting a rhombus-type of shape, with a ratio between major and minor diagonals (r_D) of 1.34. The same effect is observed for CH₃ and H adsorption, with r_D values of 1.52 and 1.43, respectively. In both cases, the Ni atom rearrangement allows the formation of Ni₃ three-fold hollow sites, where both CH₃ and H species adsorb. Lability is not observed either for methane or H adsorbed on the Ni₉/TiC cluster, yet the Ni₃ three-fold hollow site emerges when CH₃ is adsorbed, with a r_D of 1.30, hence smaller than the value of 1.52 for Ni₄/TiC. Finally, on the 3D

Ni₁₃/TiC cluster the different species energetically prefer to adsorb at the edges of the cluster.

Table 1. PBE-D3 adsorption energies (ZPE corrected, E_{ads} , in eV) of CH₄, CH₃, and H on the clean TiC(001) and Ni(111) surfaces and on several Ni_n/TiC surfaces (n = 4, 9, 13). ^a Value taken from Ref. 50 (PBE-D2), note that it does not include ZPE. ^b Values taken from Ref. 56 (PBE).

	E_{ads} /eV		
	CH ₄	CH ₃	H
Ni(111)	-0.24 ^a	-1.81 ^b	-2.77 ^b
TiC(001)	-0.25	-2.26	-2.77
Ni ₄ /TiC	-0.57	-3.12	-3.42
Ni ₉ /TiC	-0.64	-3.04	-3.32
Ni ₁₃ /TiC	-0.36	-2.83	-3.21

The CH₄ dissociation on Ni₄/TiC appears to be facilitated when starting from a vertex site with CH₃+H going to bridge sites with a calculated E_b of 0.18 eV only (see TS1 in Figure 9); a drastic reduction when compared to the case of Ni(111) implying an E_b of 1.07 eV.²⁷ This significant E_b lowering is related to the overall reaction energy going from 0.35 eV (endothermic) on the Ni(111) surface to -0.76 eV (exothermic) on Ni₄/TiC. This is as expected from the Brønsted-Evans-Polanyi (BEP)^{57,58} relationship applied to heterogeneously catalyzed reactions, as suggested by Pallasana and Neurock⁵⁹ and popularized by Nørskov *et al.*⁶⁰ Indeed, for CH₄ dissociation on the Ni₄, Ni₉ and Ni₁₃ clusters supported on TiC(001) and Ni(111), a quantitative, BEP relationship emerges when plotting E_b in front of the reaction energy as discussed in detail in a separate section.

As illustrated in Figure S9 the lability effect of the small Ni₄ cluster supported on TiC is evident. To investigate its possible effect on the CH₄ first dehydrogenation step reaction energy profile, calculations have been carried out by freezing both TiC surface and Ni cluster atoms in the most stable configuration. The resulting constrained

energy profile show a significant increase of the E_b from 0.18 eV up to 0.42 eV (see Figure S10 in SI), highlighting the important role of the lability of such small clusters in the course of CH₄ adsorption and dissociation. Interestingly, we note that r_D lowers along the reaction coordinate, from 1.34 for adsorbed CH₄, 1.19 for TS2, and 1.00 for CH₃+H products. Finally, it is worth to mention that the spin properties of Ni cluster are not negligible during the whole catalytic process. While the magnetic moment for the reactant configuration (*i.e.*, CH₄-Ni₄/TiC) is near 1, it becomes quenched down to zero for both the TS and the product configurations. These differences on the total magnetization along the CH₄ dissociation pathway are also observed for larger Ni clusters, and shown to be a key point in other catalytic processes using magnetic metal clusters, as in the course of ammonia synthesis by supported Fe clusters.⁵⁵

For the larger Ni₉ supported cluster, the most favourable path corresponds to the direct dissociation from the CH₄ molecule located on top of a vertex Ni atom to a CH₃+H configuration where CH₃ is placed on a bridge site and the H on a four-fold hollow site (see Figure S11). On this Ni₉/TiC system, E_b is just 0.25 eV, only 0.07 eV higher than corresponding value for Ni₄/TiC (0.18 eV). Interestingly, this energy barrier is still much lower than the -0.64 eV CH₄ adsorption energy on Ni₉/TiC (Table 1).

Finally, on the largest Ni₁₃ supported cluster, CH₄ and the CH₃ preferentially adsorb on a vertex of the cluster, and the released H adatom adsorbs on a three-fold hollow site of small (111) facets of the supported cluster, as shown in Figure S12. Here E_b becomes 0.38 eV, noticeably higher than the energy barriers for the smaller clusters (0.18 and 0.25 eV for Ni₄/TiC and Ni₉/TiC, respectively). Nevertheless, this value is already slightly higher than the methane adsorption energy of 0.36 eV on this Ni₁₃/TiC model system. This implies that the CH₄ dissociation criteria would not be completely fulfilled, indicating that on such larger 3D clusters the dissociation process becomes unfavourable, in agreement with the experimental observations. Note in passing by that the most stable arrangement for the CH₄-Ni_n/TiC system coincides with the most stable arrangement for the bare Ni_n/TiC clusters in all three models. Only some elongations or contractions between the Ni atoms are observed on the two-dimensional Ni₄/TiC and Ni₉/TiC models.

The synergic effect between Ni particles and the TiC(001) support, becomes more evident when comparing CH₄ adsorption energies and first dehydrogenation energy barriers to equivalent values calculated for the pristine Ni(111) and TiC(001) extended surfaces reported in Table 2. Clearly, only 2D Ni clusters supported on TiC

exhibit E_{ads} values larger than E_b energy barriers. This conclusion is further supported from total energy and Gibbs free energy profiles in Figure 9; the latter corresponding to 300 K and 1 atm (1.01325 bar) of CH_4 partial pressure. The Gibbs free energy profiles indicate that on all the studied Ni_n/TiC clusters both adsorption and dissociation processes are exergonic; contrary to the situation corresponding to Ni(111). Moreover, the smaller Ni_4/TiC and Ni_9/TiC clusters present no effective free energy barrier for CH_4 dissociation at normal conditions, confirming that small Ni particles are particularly active to trigger CH_4 dissociation at room temperature, in agreement with the experimental findings. Note also that room temperature is actually the temperature where the highest conversion is achievable, given that a rise in temperature would only place the effective energy barrier above the reactant energy limit, in accordance with experiment.

Table 2. CH_4 adsorption energies, E_{ads} , and first dehydrogenation energy barriers, E_b , on Ni_n/TiC , TiC(001) and Ni(111). All values are given in eV. ^a Ref. 50 (PBE-D2), ^b Ref. 56 (PBE). Note that present E_b values account for the ZPE which is not the case for the value for Ni(111) in Ref. 50; on the average ZPE decreases the energy barrier by 0.15 eV.

Catalyst	CH_4 E_{ads}	E_b
Ni_4/TiC	-0.57	0.18
Ni_9/TiC	-0.64	0.25
$\text{Ni}_{13}/\text{TiC}$	-0.36	0.38
TiC(001)	-0.25	1.22
Ni(111)	-0.24 ^a	1.18 ^b

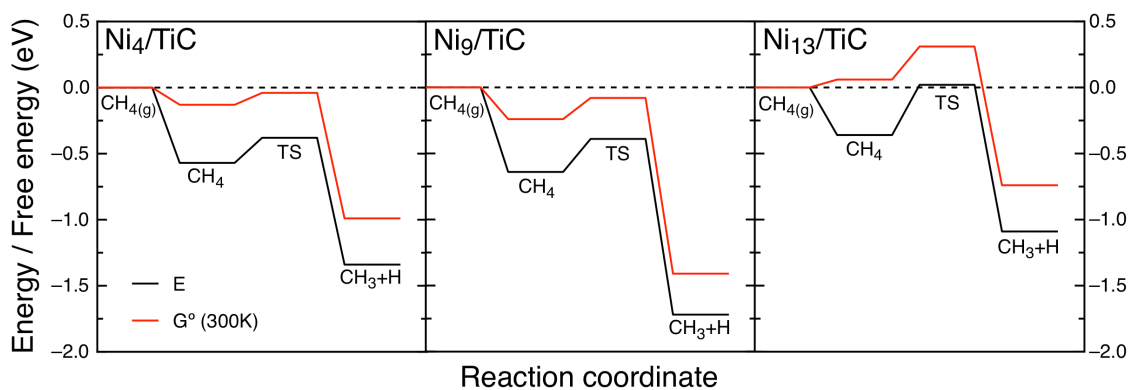


Figure 9. Total (ZPE corrected) energy profile (black lines, equivalent to the Gibbs free energy profiles at 0 K and zero CH₄ partial pressure) and at 300 K and 1 atm of CH₄ (red lines) on the three studied Ni_n/TiC(001) systems.

At this stage one may wonder whether the effect of the TiC support consists in stabilizing adsorbed methane, decreasing the dissociation energy barrier, or both. The support effect has been qualitatively studied by comparing the full energy profile of the dissociation reaction computed in two different ways: *i*) with the surface atoms and the cluster Ni atoms frozen to the most stable configuration for the clean supported cluster (black line in Figure 10), and *ii*) for the same clean cluster molecular structure but removing the TiC support (blue line in Figure 11). Obviously, in the case of CH₄ interacting with the unsupported Ni₄ cluster with the frozen structure, the ZPE corrections have not been included. The results of this computational experiment indicate that, while the energy barrier for CH₄ dissociation on the unsupported or supported Ni₄ cluster is quite similar (0.43 *versus* 0.50 eV), CH₄ adsorption on Ni₄ is no longer favoured when the TiC support is not present, a clear demonstration of the key role of the interaction between the Ni cluster and the support. The effect seems also to be linked to the planar structure of such small Ni_n clusters adopted upon interaction with the TiC(001) surface. This is in agreement with the results reported for CH₄ adsorption and dissociation on tetrahedral Ni₄ and icosahedral Ni₁₃ gas phase clusters where E_{ads} of 0.39 and 0.40 eV are smaller and E_b values of 0.44 and 0.43 eV are larger than for the supported clusters, respectively.⁶¹

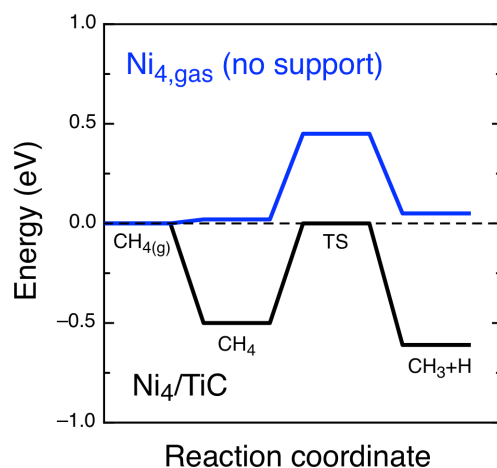


Figure 10. Energy profiles (non ZPE corrected) for CH₄ adsorption and subsequent dissociation on frozen Ni₄ cluster supported on TiC (black line) and unsupported (blue line).

Finally, we focus on the finite size effects of the three supported Ni clusters by comparing E_{ads} and E_b values with respect to an infinite array of Ni atoms forming a supported nanorod, as shown in Figure 2. The nanorod shape resembles that of a Ni₁₃/TiC cluster expanded in one [010] direction so as to generate a periodic structure with bulk-like properties. The incommensurability of the periodic Ni nanorod structure and the TiC(001) surface leads to clustering of Ni atoms and a degree of lability of the second layer of Ni atoms. On this supported nanorod model, E_{ads} is -0.49 eV, slightly smaller than the corresponding values on Ni₄/TiC and Ni₉/TiC (Table 1), yet highlighting the importance of low coordinated Ni atoms on methane adsorption as well as the effect of the support. Note, however, that the E_{ads} value for the supported nanorod is larger than that computed for the Ni₁₃/TiC cluster (-0.36 eV), which is attributed to the above-stated lability of the Ni rod compared to the rigidity of the Ni₁₃/TiC cluster. However, the important aspect is that, on the supported nanorod, the CH₄ dissociation energy barrier is 0.64 eV, much higher than the corresponding values for the finite supported clusters, and also higher than the desorption energy. The latter kinetically inhibits CH₄ dissociation, with an even more unfavourable free energy profile at working conditions of temperature and pressure (see Figure 11).

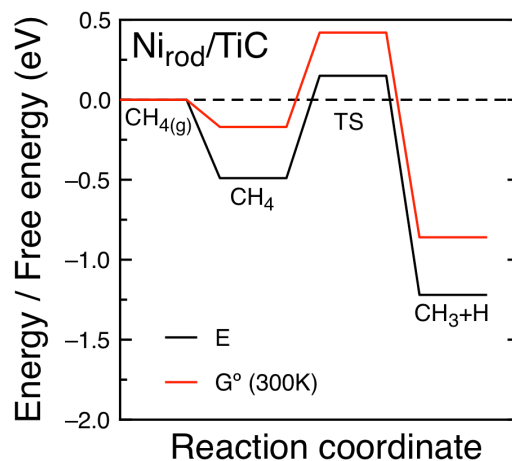


Figure 11. Total ZPE corrected energy (black lines) and Gibbs free energy at 300 K and 1 atm of CH₄ (red lines) profiles for CH₄ adsorption and dissociation on the Ni nano-rod supported on TiC(001).

Unravelling trends in C-H activation. To further investigate the chemistry involved in the activation of the C-H bond in CH₄ through its interaction with the Ni/TiC systems studied in the present work, as well as to attempt to obtain appropriate simple descriptors, we analyse in detail the relationship between the calculated values of the energy barrier for C-H activation and the corresponding energy reaction with adsorbed CH₃ and H as products. For convenience and, also, for a possible practical use of the resulting BEP relationship,^{59,60} the values not corrected by the ZPE have been used. Note, however, that the main influence of ZPE is in the adsorption energy of CH₄ which leads to an average systematic reduction of the calculated energy barriers of ~0.15 eV. Besides, the values corresponding to the Ni(111) extended surface have been included as this provides an appropriate model for the limiting case of very large supported particles. The resulting BEP plot thus constructed is presented in Figure 12, and shows a clear, linear trend. This is an interesting result since it would allow one to estimate the energy barrier for similar systems by simple interpolation and without the need to compute the vibrational frequencies of the adsorbed products. More importantly, the BEP in Figure 12 shows that the low energy barrier for the systems used in the experiments comes from the fact that the underlying carbide stabilizes the dissociation products when the supported particles are small enough. The effect gradually disappears for larger particles and almost vanishes for the supported nanorod model where the decrease in the energy barrier with respect to Ni(111) is clearly due to the presence of the low coordinated Ni atoms.

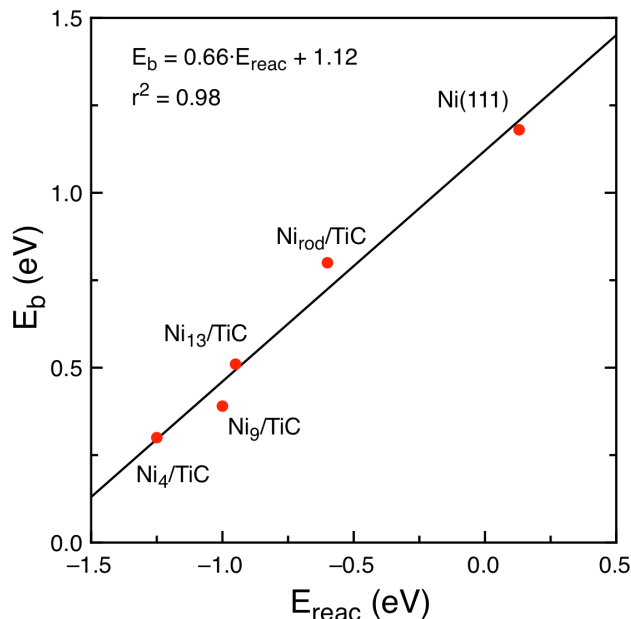


Figure 12. Energy barrier (E_b) for CH_4 to CH_3+H dissociation on the Ni/TiC systems and on Ni(111) versus the reaction energy (E_{reac}). The values used to construct the plot are reported in Table S2 and, for convenience, do not include the ZPE term.

At this point one may wonder whether the chemistry governing C-H scission in these systems bears some similarity to that exhibited by oxides and zeolites, some of which are able to dissociate CH_4 . In a recent paper, Latimer *et al.*²¹ studied trends in C-H activation for several hydrocarbons on a broad family of materials containing O atoms including, among others, oxides, zeolites and metal organic frameworks and graphene. Interestingly, they argue that the overall chemistry is governed by hydrogen affinity (E_H^f) defined as the formation energy of adsorbed hydrogen with respect to gas phase H_2O and O_2 . More specifically, these authors found that E_H^f can be used as a descriptor for predicting the formation energy of the transition state for C-H scission (E_{TS}^f) in a variety of O containing catalysts; *i.e.* that E_{TS}^f goes linear E_H^f . Moreover, they postulate that the origin of this behaviour lies in the radical-like TS character involving one site on the catalyst surface only, and, therefore, is supposed to be rather independent of the particular catalyst geometry.²¹

Inspired by this work, we adapted the definition of E_H^f and E_{TS}^f to the Ni/TiC systems studied in the present work. To this end, we define the formation energy of adsorbate i , E_i^f , referenced to the clean surface and to gas-phase H_2 and CH_4 as

$$E_i^f = U_{i+slab} - U_{slab} - \sum_j (n_j R_j) \quad (4),$$

where U_{i+slab} is the raw DFT energy of the slab with adsorbate i , U_{slab} is the raw DFT energy of the slab, n_j is the number of atomic species j in i , and R_j is the reference energy of that atomic species with the reference energies R_j for each atomic species defined as

$$R_H = \frac{1}{2}U_{H_2(g)} \quad (5),$$

$$R_C = U_{CH_4(g)} - 4R_H \quad (6),$$

where again $U_{i(g)}$ is a “raw” energy directly taken from the DFT based calculation. We note that one interesting feature of the formation energy approach (as opposed to the use of pure DFT energies) is that it does not distinguish between thermodynamic minima (adsorbed states) and saddle points (transition-states). Thus, it is possible to define the formation energy of the CH₃-H dissociation transition state, E_{TS}^f , as

$$E_{TS}^f = U_{CH_3-H+slab} - U_{slab} - R_C - 4R_H \quad (7),$$

which is related to the DFT calculated energy barrier for CH₃-H dissociation, E_b , as

$$E_b = E_{TS}^f - E_{CH_4}^f \quad (8).$$

The analysis of the E_{TS}^f versus E_H^f plots (Figure S15) shows that while the main trend in the formation energy of the TS is well captured by hydrogen affinity E_H^f descriptor, there is a considerable deviation from linearity implying that the chemical mechanism for CH₄ activation by Ni/TiC is different and does not involve the same type of radical like TS. Interestingly, plotting the natural logarithm of the raw DFT energy barrier with respect to the adsorbed hydrogen formation energy results in an almost perfect straight line as shown in Figure 13, indicating a somehow different chemistry. In the case of low-temperature methane dissociation on IrO₂(110)³¹ and Ni/CeO₂(111)⁶² a concerted mechanism has been reported where the cleavage of the first C-H bond involves simultaneous bonding interactions with a metal cation and an oxygen anion. This type of interactions cannot take place on a metal/carbide system where the C centres do not have the very high negative charge present in the O centres of an oxide (*i.e.*, carbides have a lower degree of ionicity than oxides).^{63,64} Nevertheless, the C centres in the carbide can be involved in the activation of methane by enhancing the reactivity of a supported metal or by accommodating the H and CH₃ produced by the dissociation of the hydrocarbon.

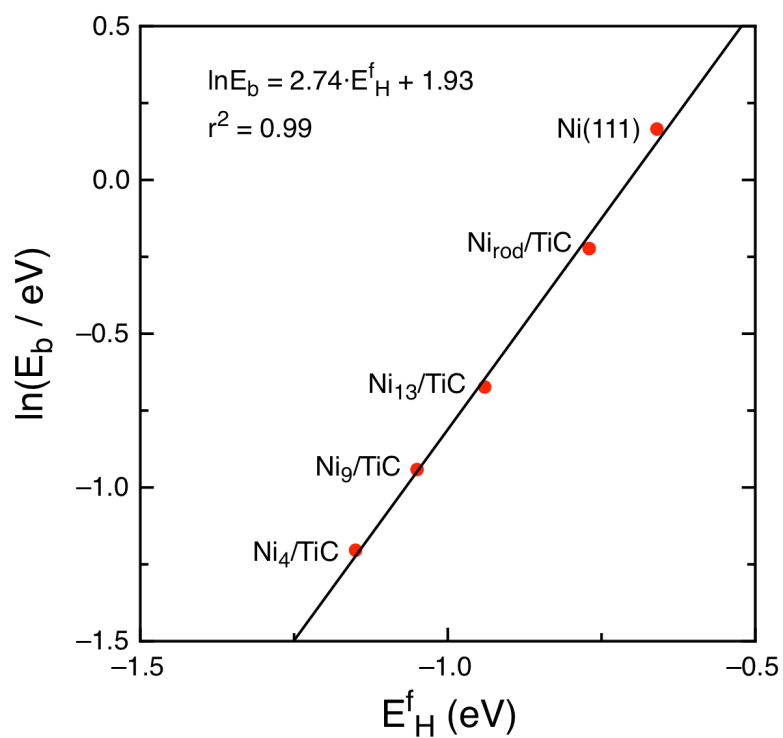


Figure 13. Logarithm of the energy barrier (E_b) for CH_4 to CH_3+H dissociation on the Ni/TiC systems and on Ni(111) versus the E_H^f . For convenience, the values used to construct the plot do not include the ZPE term.

CONCLUSIONS

The interaction of methane with pristine Ni(111) and TiC(001) surfaces is very weak. In contrast, a series of XPS experiments for 0.2 ML of Ni supported on a TiC(001) single crystal point to CH₄ adsorption and decomposition at room temperature and low partial pressures of the hydrocarbon. This unexpected, exciting and technologically relevant result has been explained by means of DFT based calculations on models of Ni clusters and nanorods supported on TiC(001) surface. These calculations confirm that small 2D supported Ni clusters are responsible for the observed catalytic behaviour featuring adsorption energies up to -0.64 eV, thus allowing for CH₄ adsorption at room temperature. At the same time, on the supported clusters, C-H bond scission energy barriers become smaller than the CH₄ adsorption energies, and can be as low as 0.18 eV. The lability of such 2D few-atom Ni clusters, together with the interaction with the support, appear to promote methane adsorption and low-energy barrier decomposition into CH₃ and H. These features are lost for larger 3D supported Ni clusters indicating that the mere existence of low coordinated sites does is not sufficient to trigger C-H scission before desorption takes place.

Our results for a range of Ni/TiC systems, including extended Ni(111) surface as a limiting case, show that a BEP relationship holds for the C-H scission. This indicates that the interaction between the metal and the underlying carbide support stabilizes the dissociation products with a concomitant decrease of the energy barrier involved in this elementary step. Moreover, it is found that the adsorbed hydrogen formation energy E_H^f constitutes a very good descriptor for methane activation on these Ni-based catalysts. However, E_H^f appears to be directly related to the logarithm of the raw energy barrier E_b for CH₄ dissociation and not to the TS formation energy (E_{TS}^f) as in the case of oxides and zeolites²¹ implying that a different chemistry is involved.

The present results open the way for the preparation of a new family of active materials for methane activation and conversion under mild conditions, thus widening the applications of existing natural gas resources.

CONFLICTS OF INTEREST

The authors declare no conflict of interest.

ASSOCIATED CONTENT

Supporting Information

The following Supporting Information is available free of charge on the ACS Publications website at DOI:

- S1. Computational details
 - S2. Adsorption energies on clean TiC
 - S3. Transition state for CH₄ dissociation on clean TiC
 - S4. Adsorption energies on supported Ni clusters
 - S5. Transition states for CH₄ dissociation on supported Ni clusters
 - S6. Adsorption energies on the supported Ni nanorod
 - S7. Transition state for CH₄ dissociation on on the supported Ni nanorod
 - S8. Kinetic parameters and free energies
 - S9. Details on the calculation of descriptors for C-H activation
- References

ACKNOWLEDGEMENTS

This manuscript has been authored by employees of Brookhaven Science Associates, LLC under Contract No. DE-SC0012704 with the U.S. Department of Energy. The research carried out at the *Universitat de Barcelona* was supported by the Spanish MINECO/FEDER CTQ2015-64618-R and, in part, by *Generalitat de Catalunya* (grants 2017SGR13 and XRQTC). H.P.G. acknowledges financial support from *Generalitat de Catalunya* predoctoral FI-DGR-2015 grant. J.J.P. thanks the Spanish MINECO for *Ayuda para la formación de doctores* contract (BES-2016-78816). F.V. thanks the MINECO for a postdoctoral *Ramón y Cajal* (RyC) research contract (RYC-2012-10129), and F.I. acknowledges additional support from the 2015 ICREA Academia Award for Excellence in University Research. Financial support from Spanish MINECO through the Excellence *María de Maeztu* program (grant MDM-2017-0767) is also fully acknowledged. Authors are thankful for the computational time provided at Marenostrum-IV supercomputer at the Barcelona Supercomputing Centre (BSC) through the grants QCM-2018-2-0006 and QCM-2018-1-0032 awarded by the *Red Española de Supercomputacion* (RES).

References

- ¹ Feichter, J.; Schurath, U.; Zellner, R. Luftchemie und Klima. *Chem. Unserer Zeit* **2007**, *41*, 138–150.
- ² Spahni, R.; Chappellaz, J.; Stocker, T. F.; Louergue, L.; Hausammann, G.; Kawamura, K.; Flückiger, J.; Schwander, J.; Raynaud, D.; Masson-Delmotte, V.; Jouzel, J. Atmospheric Methane and Nitrous Oxide of the Late Pleistocene from Antarctic Ice Cores. *Science* **2005**, *310*, 1317–1321.
- ³ Grunwald, M.; Dellwig, O.; Beck, M.; Dippner, J. W.; Freund, J. A.; Kohlmeier, C.; Schnetger, B.; Brumsack, H.-J. Methane in the Southern North Sea: Sources, Spatial Distribution and Budgets. *Estuar., Coast. Shelf Sci.* **2009**, *81*, 445–456.
- ⁴ Denman, K. L.; Brasseur, G.; Chidthaisong, A.; Ciais, P.; Cox, P. M.; Dickinson, R. E.; Hauglustaine, D.; Heinze, C.; Holland, E.; Jacob, D.; Lohmann, U.; Ramachandran, S.; da Silva Dias, P. L.; Wofsy S. C.; Zhang, X. 2007: Couplings Between Changes in the Climate System and Biogeochemistry. In *Climate Change 2007: The Physical Science Basis. Contribution of Working Group I to the Fourth Assessment Report of the Intergovernmental Panel on Climate Change* Eds.: Solomon, S.; Qin, D.; Manning, M.; Chen, Z.; Marquis, M.; Averyt, K. B.; Tignor M.; Miller, H. L. Cambridge University Press, Cambridge, United Kingdom and New York, NY, USA.
- ⁵ Louergue, L.; Schilt, A.; Spahni, R.; Masson-Delmotte, V.; Blunier, T.; Lemieux, B.; Barnola, J.-M.; Raynaud, D.; Stocker, T. F.; Chappellaz, J. Orbital and Millennial-Scale Features of Atmospheric CH₄ over the Past 800,000 Years. *Nature* **2008**, *453*, 383–386.
- ⁶ Thornton, P. K. Livestock Production: Recent Trends, Future Prospects. *Philos. Trans. R. Soc. Lond. B Biol. Sci.* **2010**, *365*, 2853–2867.
- ⁷ Tang, P.; Zhu, Q.; Wu, Z.; Ma, D. Methane Activation: The Past and Future. *Energy Environ. Sci.* **2014**, *7*, 2580–2591.
- ⁸ Bousquet, P.; Ciais, P.; Miller, J. B.; Dlugokencky, E. J.; Hauglustaine, D. A.; Prigent, C.; Van der Werf, G. R.; Peylin, P.; Brunke, E.-G.; Carouge, C.; Langenfelds, R. L.; Lathière, J.; Papa, F.; Ramonet, M. Schmidt, M.; Steele, L. P.; Tyler, S. C.; White J. Contribution of Anthropogenic and Natural Sources to Atmospheric Methane Variability. *Nature* **2006**, *443*, 439–443.
- ⁹ Leung, D. Y. C.; Caramanna, G.; Maroto-Valer, M. M. An Overview of Current Status of Carbon Dioxide Capture and Storage Technologies. *Renew. Sust. Energ. Rev.* **2014**, *39*, 426-443.

- ¹⁰ Markewitz, P.; Kuckshinrichs, W.; Leitner, W.; Linssen, J.; Zapp, P.; Bongartz, R.; Schreiber, A.; Müller, T. E. Worldwide Innovations in the Development of Carbon Capture Technologies and the Utilization of CO₂. *Energy Environ. Sci.* **2012**, *5*, 7281–7305.
- ¹¹ Besenbacher, F.; Chorkendoff, I.; Clausen, B. S.; Hammer, B.; Molenbroek, A. M.; Nørskov, J. K.; Stensgaard, I. Design of a Surface Alloy Catalyst for Steam Reforming. *Science*, **1998**, *279*, 1913–1915.
- ¹² Choudhary, T. V.; Choudhary, V. R. Energy-Efficient Syngas Production through Catalytic Oxy-Methane Reforming Reactions. *Angew. Chem. Int. Ed.* **2008**, *47*, 1828–1847.
- ¹³ Tomishige, K.; Chen, Y.; Fujimoto, K. Studies on Carbon Deposition in CO₂ Reforming of CH₄ over Nickel–Magnesia Solid Solution Catalysts. *J. Catal.* **1999**, *181*, 91–103.
- ¹⁴ Bradford, M. C. J.; Vannice, M. A. CO₂ Reforming of CH₄. *Catal. Rev.* **1999**, *41*, 1–42.
- ¹⁵ Froment, G. F. Production of Synthesis Gas by Steam- and CO₂-Reforming of Natural Gas. *J. Mol. Catal. A: Chem.* **2000**, *163*, 147–156.
- ¹⁶ Hook, J. P. V. Methane-Steam Reforming. *Catal. Rev.* **1980**, *21*, 1–51.
- ¹⁷ Dissanayake, D.; Rosynek, M. P.; Kharas, K. C. C.; Lunsford, J. H. Partial Oxidation of Methane to Carbon Monoxide and Hydrogen over a Ni/Al₂O₃ Catalyst. *J. Catal.* **1991**, *132*, 117–127.
- ¹⁸ Hickman, D. A.; Schmidt, L. D. Production of Syngas by Direct Catalytic Oxidation of Methane. *Science* **1993**, *259*, 343–346.
- ¹⁹ Choudhary, V. R.; Rajput, A. M.; Prabhakar, B. Nonequilibrium Oxidative Conversion of Methane to CO and H₂ with High Selectivity and Productivity over Ni/Al₂O₃ at Low Temperatures. *J. Catal.* **1993**, *13*, 326–328.
- ²⁰ Wei, J.; Iglesia, E. Isotopic and Kinetic Assessment of the Mechanism of Reactions of CH₄ with CO₂ or H₂O to Form Synthesis Gas and Carbon on Nickel Catalysts. *J. Catal.* **2004**, *224*, 370–383.
- ²¹ Latimer, A. A.; Kulkarni, A. R.; Aljama, H.; Montoya, J. H.; Yoo, J. S.; Tsai, C.; Abild-Pedersen, F.; Studt, F.; Nørskov, J. K. Understanding Trends in C-H Bond Activation in Heterogeneous Catalysis. *Nat. Mater.* **2017**, *16*, 225–229.

- ²² Fung, V.; Tao, F.; Jiang, D. Low-Temperature Activation of Methane on Doped Single Atoms: Descriptor and Prediction. *Phys. Chem. Chem. Phys.* **2018**, *20*, 22909–22914.
- ²³ Tomkins, P.; Ranocchiari, M.; van Bokhoven, J. A. Direct Conversion of Methane to Methanol under Mild Conditions over Cu-Zeolites and Beyond. *Acc. Chem. Res.* **2017**, *50*, 418–425.
- ²⁴ Li, J.; Zhou, S.; Zhang, J.; Schlangen, M.; Weiske, T.; Usharani, D.; Shaik, S.; Schwarz, H. Electronic Origins of the Variable Efficiency of Room-Temperature Methane Activation by Homo- and Heteronuclear Cluster Oxide Cations $[XYO_2]^+$ (X, Y = Al, Si, Mg): Competition between Proton-Coupled Electron Transfer and Hydrogen-Atom Transfer. *J. Am. Chem. Soc.* **2016**, *138*, 7973–7981.
- ²⁵ Baek, J.; Rungtaweeworanit, B.; Pei, X.; Park, M.; Fakra, S. C.; Liu, Y. S.; Matheu, R.; Alshimiri, S. A.; Alshehri, S.; Trickett, C. A.; Somorjai, G. A.; Yaghi, O. M. Bioinspired Metal–Organic Framework Catalysts for Selective Methane Oxidation to Methanol. *J. Am. Chem. Soc.* **2018**, *140*, 18208–18216.
- ²⁶ Choudhary, T. V.; Aksoylu, E.; Goodman, D. W. Nonoxidative Activation of Methane. *Catal. Rev.* **2003**, *45*, 151–203.
- ²⁷ Nave, S.; Jackson, B. Methane Dissociation on Ni(111) and Pt(111): Energetic and Dynamical Studies. *J. Chem. Phys.* **2009**, *130*, 054701.
- ²⁸ Bisson, R.; Sacchi, M.; Dang, T. T.; Yoder, B.; Maroni, P.; Beck, R. D. State-Resolved Reactivity of $CH_4(2v_3)$ on Pt(111) and Ni(111): Effects of Barrier Height and Transition State Location. *J. Phys. Chem. A*, **2007**, *111*, 12679–12683.
- ²⁹ González, S.; Viñes, F.; García, J. F.; Erazo, Y.; Illas, F. A DF-VdW Study of the CH_4 Adsorption on Different Ni Surfaces. *Surf. Sci.* **2014**, *625*, 64–68.
- ³⁰ Kozlov, S. M.; Neyman, K. M. Insights from Methane Decomposition on Nanostructured Palladium. *J. Catal.* **2016**, *337*, 111–121.
- ³¹ Liang, Z.; Li, T.; Kim, M.; Asthagiri, A.; Weaver, J. F. Low-Temperature Activation of Methane on the $IrO_2(110)$ Surface. *Science* **2017**, *356*, 299–303.
- ³² Liu, K.; Yuan, C.; Zou, Q.; Xie, Z.; Yan, X. Self-Assembled Zinc/Cystine-Based Chloroplast Mimics Capable of Photoenzymatic Reactions for Sustainable Fuel Synthesis. *Angew. Chem. Int. Ed.* **2017**, *56*, 7876–7880.
- ³³ Park, J. B.; Graciani, J.; Evans, J.; Stacchiola, D.; Ma, S.; Liu, P.; Nambu, A.; Sanz, J. F.; Hrbek, J.; Rodriguez, J. A. High Catalytic Activity of $Au/CeO_x/TiO_2(110)$

Controlled by the Nature of the Mixed-Metal Oxide at the Nanometer Level. *Proc. Natl. Acad. Sci.* **2009**, *106*, 4975–4980.

³⁴ Rodriguez, J. A.; Liu, P.; Hrbek, J.; Pérez, M.; Evans, J. Water–Gas Shift Activity of Au and Cu Nanoparticles Supported on Molybdenum Oxides. *J. Mol. Catal. A: Chem.* **2008**, *281*, 59–65.

³⁵ Yang, Y.; Evans, J.; Rodriguez, J. A.; White, M. G.; Liu, P. Fundamental Studies of Methanol Synthesis from CO₂ Hydrogenation on Cu(111), Cu Clusters, and Cu/ZnO (000 $\bar{1}$). *Phys. Chem. Chem. Phys.* **2010**, *12*, 9909–9917.

³⁶ Rodriguez, J. A.; Evans, J.; Feria, L.; Vidal, A. B.; Liu, P.; Nakamura, K.; Illas, F. CO₂ Hydrogenation on Au/TiC, Cu/TiC, and Ni/TiC Catalysts: Production of CO, Methanol, and Methane. *J. Catal.* **2013**, *307*, 162–169.

³⁷ Frantz, P. P.; Didziulis, S. V.; Detailed Spectroscopic Studies of Oxygen on Metal Carbide Surfaces. *Surf. Sci.* **1998**, *412/413*, 384–396.

³⁸ Rodriguez, J. A.; Kuhn, M. Electronic Properties of Gold on Mo(110): $d \rightarrow s,p$ Charge Redistribution and Valence Band Shifts. *Surf. Sci.* **1995**, *330*, L657–L664.

³⁹ Rodriguez, J. A.; Liu, P.; Takahashi, Y.; Nakamura, K.; Viñes, F.; Illas, F.; Desulfurization of Thiophene on Au/TiC(001): Au-C Interactions and Charge Polarization. *J. Amer. Chem. Soc.* **2009**, *131*, 8595–8602.

⁴⁰ Rodriguez, J. A.; Ramirez, J. P.; Asara, G. G.; Viñes, F.; Evans, J.; Liu, P.; Ricart, J. M.; Illas, F. Charge Polarization at a Au-TiC Interface and the Generation of Highly Active and Selective Catalysts for the Low-Temperature Water-Gas Shift Reaction. *Angew. Chem. Int. Ed.* **2014**, *53*, 11270–11274.

⁴¹ Vidal, A. B.; Feria, L.; Evans, J.; Takahashi, Y.; Liu, P.; Nakamura, K.; Illas, F.; Rodriguez, J. A. CO₂ Activation and Methanol Synthesis on Novel Au/TiC and Cu/TiC Catalysts. *J. Phys. Chem. Lett.* **2012**, *3*, 2275–2280.

⁴² Perdew, J. P.; Burke, K.; Ernzerhof, M. Generalized Gradient Approximation Made Simple. *Phys. Rev. Lett.* **1996**, *77*, 3865–3868

⁴³ Grimme, S.; Antony, J.; Ehrlich, S.; Krieg, S. A Consistent and Accurate Ab Initio Parametrization of Density Functional Dispersion Correction (DFT-D) for the 94 Elements H–Pu. *J. Chem. Phys.* **2010**, *132*, 154104.

⁴⁴ Henkelman, G.; Uberuaga, B. P.; Jónsson, H. A Climbing Image Nudged Elastic Band Method for Finding Saddle Points and Minimum Energy Paths. *Phys. Rev. B* **2000**, *113*, 9901–9904.

- ⁴⁵ Larsen, A. H.; Mortensen, J. J.; Blomqvist, J.; Castelli, I. E.; Christensen, R.; Dułak, M.; Friis, J.; Groves, M. N.; Hammer, B.; Hargus, C.; Hermes, E. D.; Jennings P. C.; Jensen, P. B.; Kermode, J.; Kitchin, J. R.; Kolsbjerg, E. L.; Kubal, J.; Kaasbjerg, K.; Lysgaard, S.; Maronsson, J. B.; Maxson, T.; Olsen, T.; Pastewka, L.; Peterson, A.; Rostgaard, C.; Schiøtz, J.; Schütt, O.; Strange, M.; K. S.; Vegge, T.; Vilhelmsen, L.; Walter, M.; Zeng, Z.; Jacobsen, K. W. The Atomic Simulation Environment—a Python Library for Working with Atoms. *J. Phys. Condens. Matter.* **2017**, *29*, 273002.
- ⁴⁶ Smidstrup, S.; Pedersen, A.; Stokbro, K.; Jónsson, H. Improved Initial Guess for Minimum Energy Path Calculations. *J. Chem. Phys.* **2014**, *140*, 214106.
- ⁴⁷ Rogal, J.; Reuter, K. *Ab Initio Atomistic Thermodynamics for Surfaces: A Primer in Experiment, Modeling and Simulation of Gas- Surface Interactions for Reactive Flows in Hypersonic Flights*. Educational Notes. Neuilly-sur-Seine, France (2007).
- ⁴⁸ Kresse, G.; Furthmüller, J. Efficient Iterative Schemes for Ab Initio Total-Energy Calculations Using a Plane-Wave Basis Set. *Phys. Rev. B* **1996**, *54*, 11169–11186.
- ⁴⁹ Kunkel, C.; Viñes, F.; Illas, F. Biogas Upgrading by Transition Metal Carbides. *ACS Appl. Energy Mater.* **2018**, *1*, 43-47.
- ⁵⁰ Li, K.; He, C.; Jiao, M.; Wang, Y.; Wu, Z. A First-Principles Study on the Role of Hydrogen in Early Stage of Graphene Growth during the CH₄ Dissociation on Cu(111) and Ni(111) Surfaces. *Carbon* **2014**, *74*, 255-265.
- ⁵¹ Rodriguez, J. A.; Liu, P.; Viñes, F.; Illas, F.; Takahashi, Y.; Nakamura, K. Dissociation of SO₂ on Au/TiC(001): Effects of Au–C Interactions and Charge Polarization. *Angew. Chem. Int. Ed.* **2008**, *47*, 6685-6689.
- ⁵² Rodriguez, J. A.; Illas, F. Activation of Noble Metals on Metal-Carbide Surfaces: Novel Catalysts for CO Oxidation, Desulfurization and Hydrogenation Reactions, *Phys. Chem. Chem. Phys.*, **2012**, *14*, 427-438
- ⁵³ Rodriguez, J. A.; Viñes, F.; Illas, F. Adsorption of Gold on TiC(001): Au–C Interactions and Charge Polarization. *J. Chem. Phys.* **2007**, *127*, 211102.
- ⁵⁴ Gomez, T.; Florez, E.; Rodriguez, J. A.; Illas, F. Reactivity of Transition Metals (Pd, Pt, Cu, Ag, Au) toward Molecular Hydrogen Dissociation: Extended Surfaces versus Particles Supported on TiC(001) or Small Is Not Always Better and Large Is Not Always Bad. *J. Phys. Chem. C* **2011**, *115*, 11666–11672.
- ⁵⁵ Liu, J.; Ma, X.; Wang, Y.; Xiao, H.; Li, J. Heterogeneous Fe₃ Single-Cluster Catalyst for Ammonia Synthesis via an Associative Mechanism. *Nat Commun.* **2018**, *8*, 1610.

- ⁵⁶ Liu, H.; Yan, R.; Zhang, R.; Wang, B.; Xie, K. A DFT Theoretical Study of CH₄ Dissociation on Gold-Alloyed Ni(111) Surface. *J. Nat. Gas Chem.* **2011**, *20*, 611–617.
- ⁵⁷ Brønsted, J. N. Acid and Basic Catalysis. *Chem. Rev.*, **1928**, *5*, 231–338.
- ⁵⁸ Evans, M. G.; Polanyi, M. Inertia and Driving Force of Chemical Reactions. *Trans. Faraday Soc.* **1938**, *34*, 11–24.
- ⁵⁹ Pallassana, V.; Neurock, M. Electronic Factors Governing Ethylene Hydrogenation and Dehydrogenation Activity of Pseudomorphic PdML/Re(0001), PdML/Ru(0001), Pd(111), and PdML/Au(111) Surfaces. *J. Catal.* **2000**, *191*, 301–317
- ⁶⁰ Nørskov, J. K.; Studt, F.; Abild-Pedersen, F.; Bligaard, T. *Fundamental Concepts in Heterogeneous Catalysis*, John Wiley & Sons, Inc., 2014, ISBN: 978-1-118-88895-7.
- ⁶¹ Liu, B.; Lusk, M. T.; Ely, J. F. Influence of Nickel Catalyst Geometry on the Dissociation Barriers of H₂ and CH₄: Ni₁₃ versus Ni(111). *J. Phys. Chem. C* **2009**, *113*, 13715–13722.
- ⁶² Lustemberg, P. G.; Ram, G., P. J.; Liu, Z.; Guti and Ni(111) Grinter, D. G.; Carrasco, J.; Senanayake, S. D.; Rodriguez, J. A.; Ganduglia-Pirovano, M. V. Room-Temperature Activation of Methane and Dry Re-Forming with CO₂ on Ni-CeO₂(111) Surfaces: Effect of Ce³⁺ Sites and Metal-Support Interactions on C-H Bond Cleavage *ACS Catal.* **2016**, *6*, 8184–8191.
- ⁶³ Oyama, S. T. *The Chemistry of Transition Metal Carbides and Nitrides*; Springer Netherlands, 1996.
- ⁶⁴ Hwu, H. H.; Chen, J. G. Surface Chemistry of Transition Metal Carbides. *Chem. Rev.* **2005**, *105*, 185

Graphic for TOC

